Published online: May 8, 2017

Article

SOURCE DATA | TRANSPARENT PROCESS

EMBO reports

TREM2 deficiency impairs chemotaxis and microglial responses to neuronal injury

Fargol Mazaheri[1], Nicolas Snaidero[2,3], Gernot Kleinberger[4,5], Charlotte Madore[6], Anna Daria[5], Georg Werner[5], Susanne Krasemann[7], Anja Capell[5], Dietrich Trümbach[8], Wolfgang Wurst[1,4,8,9], Bettina Brunner[1], Sebastian Bultmann[10], Sabina Tahirovic[1], Martin Kerschensteiner[3,4], Thomas Misgeld[1,2,4], Oleg Butovsky[6] & Christian Haass[1,4,5,*]

Abstract

Sequence variations in the triggering receptor expressed on myeloid cells 2 (TREM2) have been linked to an increased risk for neurodegenerative disorders such as Alzheimer's disease and frontotemporal lobar degeneration. In the brain, TREM2 is predominantly expressed in microglia. Several disease-associated TREM2 variants result in a loss of function by reducing microglial phagocytosis, impairing lipid sensing, preventing binding of lipoproteins and affecting shielding of amyloid plaques. We here investigate the consequences of TREM2 loss of function on the microglia transcriptome. Among the differentially expressed messenger RNAs in wild-type and Trem2$^{-/-}$ microglia, gene clusters are identified which represent gene functions in chemotaxis, migration and mobility. Functional analyses confirm that loss of TREM2 impairs appropriate microglial responses to injury and signals that normally evoke chemotaxis on multiple levels. In an *ex vivo* organotypic brain slice assay, absence of TREM2 reduces the distance migrated by microglia. Moreover, migration towards defined chemo-attractants is reduced upon ablation of TREM2 and can be rescued by TREM2 re-expression. *In vivo*, microglia lacking TREM2 migrate less towards injected apoptotic neurons, and outgrowth of microglial processes towards sites of laser-induced focal CNS damage in the somatosensory cortex is slowed. The apparent lack of chemotactic stimulation upon depletion of TREM2 is consistent with a stable expression profile of genes characterizing the homoeostatic signature of microglia.

Keywords Alzheimer's disease; chemotaxis; microglia; neurodegeneration; TREM2

Subject Categories Immunology; Molecular Biology of Disease; Neuroscience

DOI 10.15252/embr.201743922 | Received 10 January 2017 | Revised 27 March 2017 | Accepted 31 March 2017 | Published online 8 May 2017

EMBO Reports (2017) 18: 1186–1198

Introduction

Neurodegenerative diseases share common pathological and mechanistic principles. The most obvious common denominator are insoluble deposits formed by misfolded proteins, which are usually highly expressed in affected cells or in affected areas of the central nervous system (CNS) [1]. Furthermore, for several neurodegenerative diseases, evidence exists that soluble oligomers, which may be rather stable intermediates of the aggregation process of amyloidogenic proteins, are the executers of neurotoxicity [2]. Onset and progression of individual neurodegenerative diseases are also driven by shared seeding and spreading mechanisms, which were originally described and thought to be specific to prion disorders [3]. However, the most commonly shared pathological principle of basically all neurodegenerative diseases and many other neurological disorders is gliosis associated with an inflammatory response [4]. The critical role of the inflammatory response in neurodegeneration is strongly supported by the genetic linkage of sequence variants in the triggering receptor expressed on myeloid cells 2 (TREM2), which are associated with an increased risk for several neurodegenerative disorders including Alzheimer's disease (AD), frontotemporal lobar degeneration (FTLD), Parkinson's disease, FTLD-like syndrome and Nasu–Hakola disease [5–13]. Within the nervous system, TREM2 is predominantly expressed in microglia [14,15], the resident immune cells of the brain. Microglia are known to rapidly respond to neuronal insults and pathological protein deposits in the brain by

1 German Center for Neurodegenerative Diseases (DZNE) Munich, Munich, Germany
2 Institute of Neuronal Cell Biology, Technical University Munich, Munich, Germany
3 Institute for Clinical Neuroimmunology, Biomedical Center (BMC) and University Hospital, Ludwig-Maximilians-Universität München, Munich, Germany
4 Munich Cluster for Systems Neurology (SyNergy), Munich, Germany
5 Biomedical Center (BMC), Biochemistry, Ludwig-Maximilians Universität München, Munich, Germany
6 Ann Romney Center for Neurologic Diseases, Department of Neurology, Brigham and Women's Hospital, Harvard Medical School, Boston, MA, USA
7 Institute for Neuropathology, University Medical Center Hamburg-Eppendorf, Hamburg, Germany
8 Institute of Developmental Genetics, Helmholtz Zentrum München, Neuherberg, Germany
9 Developmental Genetics, Technical University Munich-Weihenstephan, Neuherberg, Germany
10 Department of Biology and Center for Integrated Protein Science Munich (CIPSM), Ludwig Maximilians-Universität München, Munich, Germany
*Corresponding author. Tel: +49 89 4400 46549; E-mail: christian.haass@mail03.med.uni-muenchen.de

increased chemotactic migration, cytokine release, phagocytosis and proliferation (for review see [16]). TREM2 is a type-1 transmembrane protein, which is shed on the cell surface [17,18]. Certain disease-associated sequence variants, which are located in the immunoglobulin-like domain of TREM2, affect correct folding and lead to the retention of the misfolded protein within the endoplasmic reticulum [17] and consequently a reduction of its cellular functions such as phagocytosis, proliferation, pro-survival signalling, lipid sensing, ApoE binding and release of cytokines [17,19–23]. Lack of cell surface TREM2 can be assessed in humans by quantitative analysis of soluble TREM2 (sTREM2) within biological fluids [17,24–26]. Indeed, patients with a homozygous TREM2 p.T66M mutation have no detectable sTREM2 in blood and cerebrospinal fluid (CSF) [17,25]. Moreover, increased levels of CSF sTREM, as it is observed in early stages of AD, may reflect a protective activation response of microglia [24,27]. Neuropathological consequences of a loss of TREM2 function have been detected in mouse models for AD-like plaque pathology. In such models, reduced Trem2 function consistently led to reduced clustering of microglia around amyloid plaques [28–31]. As a consequence, a diffuse type of amyloid plaques accumulates, which may be due to reduced phagocytic clearance of the plaque halo [29]. Alternatively, reduced barrier function may lead to enhanced amyloid plaque growth and as a consequence increased disease progression [30]. Indeed, such diffuse plaques, which accumulate in mice deficient of Trem2, are associated with severe axonal dystrophy [29,30]. Together, these findings suggest that disease-associated TREM2 mutations affect disease onset due to a loss of function. We therefore compared the transcriptome of microglia derived from wild-type (WT) or Trem2 knockout ($Trem2^{-/-}$) mice with the aim to identify gene clusters pinpointing to a pivotal TREM2-dependent function.

Results

Trem2 deficiency affects expression profiles of genes involved in chemotaxis

To address the impact of a Trem2 loss of function on microglial gene expression, we isolated microglia from brains of adult WT and $Trem2^{-/-}$ mice by fluorescence-activated cell sorting (FACS) using anti-FCRLS and anti-CD11b antibodies [15]. Microglia were analysed for changes in their transcriptional profile using NanoString-based chips containing 482 microglia-enriched genes [15]. Gene expression levels in each sample were normalized against the geometric mean of six housekeeping genes including *Cltc*, *Gapdh*, *Gusb*, *Hprt1*, *Pgk1* and *Tubb5*. Within the set of 482 genes analysed, more than half them were unchanged, 88 were upregulated and 34 were downregulated (Dataset EV1). A scatter plot of the normalized and averaged gene expression levels from $Trem2^{-/-}$ mice against WT mice demonstrates that none of the genes show a fold change greater than two but several genes indicate a fold change of < 0.5 (Fig 1A). We then performed a gene ontology pathway analysis. This revealed clusters of dysregulated genes (Fig 1B) that were associated with chemotactic motility, wounding and cytokine response (Table 1 and Dataset EV3). Literature searches pointed out that specifically, the downregulated genes *Ccl2*, *Il1b*, *Tnf* and *Spp1* of the category cell motility (Table 1) are putative direct targets of Trem2 [20,32,33]. Furthermore, application of pathway enrichment analysis separately to significantly up- and downregulated genes from the NanoString-based screen revealed that in particular, downregulated genes contribute to chemotaxis and migration (compare the top significant functional categories of Datasets EV1 and EV2). Significantly downregulated genes (e.g. *Il1b*, *Vegfa*) involved in chemotaxis and migration are highlighted in Fig EV1.

To validate a potential impact of Trem2 loss of function on chemotactic migration, we used independent *in vitro*, *ex vivo* and *in vivo* approaches.

Trem2 deficiency impairs chemotaxis in organotypic slice cultures

First, we utilized our recently established *ex vivo* assay [34] of co-culturing of young (P5) WT and old (12–14 months) APPPS1 [35] organotypic brain slices. This assay allows the quantitative investigation of chemotactic migration of young microglia towards injured and dying tissue derived from APPPS1 mice (Fig 2A). Microglia were visualized using Cx3cr1-GFP [36] as a microglia reporter as well as staining of CD68 (Fig 2A) and analysed after 7 days *in vitro* (DIV). Baseline migration of CD68-positive cells was observed, when slices from young WT mice were cultured alone, and was significantly reduced when brain slices were prepared from young $Trem2^{-/-}$ mice (Fig 2B; for quantification see Fig 2D). Upon co-culturing of young WT slices with brain slices derived from old APPPS1 mice, the distance migrated by CD68-positive cells increased significantly (Fig 2C; for quantification see Fig 2D). This is in striking contrast to CD68-positive cells devoid of Trem2. Here, the distance migrated was significantly less and no different to that observed when young tissue was cultured alone (Fig 2C and D). This suggests that the old dying tissue may provide chemotactic signals, which attract WT- but not Trem2-deficient microglia and

Figure 1. Disturbed expression of gene clusters involved in chemotaxis in the absence of Trem2.

A Scatter plot of the normalized and averaged log2 gene expression level of $Trem2^{-/-}$ mice (KO) against wild-type (WT) samples. The upper red line corresponds to a fold change of 2 while the lower red line indicates a fold change of 0.5.

B Gene expression profile of the normalized log2 transformed levels (for genes with $P < 0.05$ after Student's *t*-test and FDR < 0.158) from the NanoString-based chips represented by a heat map. For generation of the heat map, the heatmap.2 function within the gplots package of R statistical software was used. Hierarchical clustering by the hclust function (method = "complete") was applied to group experimental conditions (columns) as well as intensities of genes (rows) for the heat map. Rows are scaled and represented as *z*-score. A dendrogram is shown only for the columns. For the assignment of genes to functional categories at the right site of the heat map, the enrichment analysis of the GeneRanker was used but also a pathway analysis with help of the Pathway Studio software (Copyright 2014, Elsevier) as well as manual literature searches. WT $N = 5$, $Trem2^{-/-}$ $N = 7$.

Source data are available online for this figure.

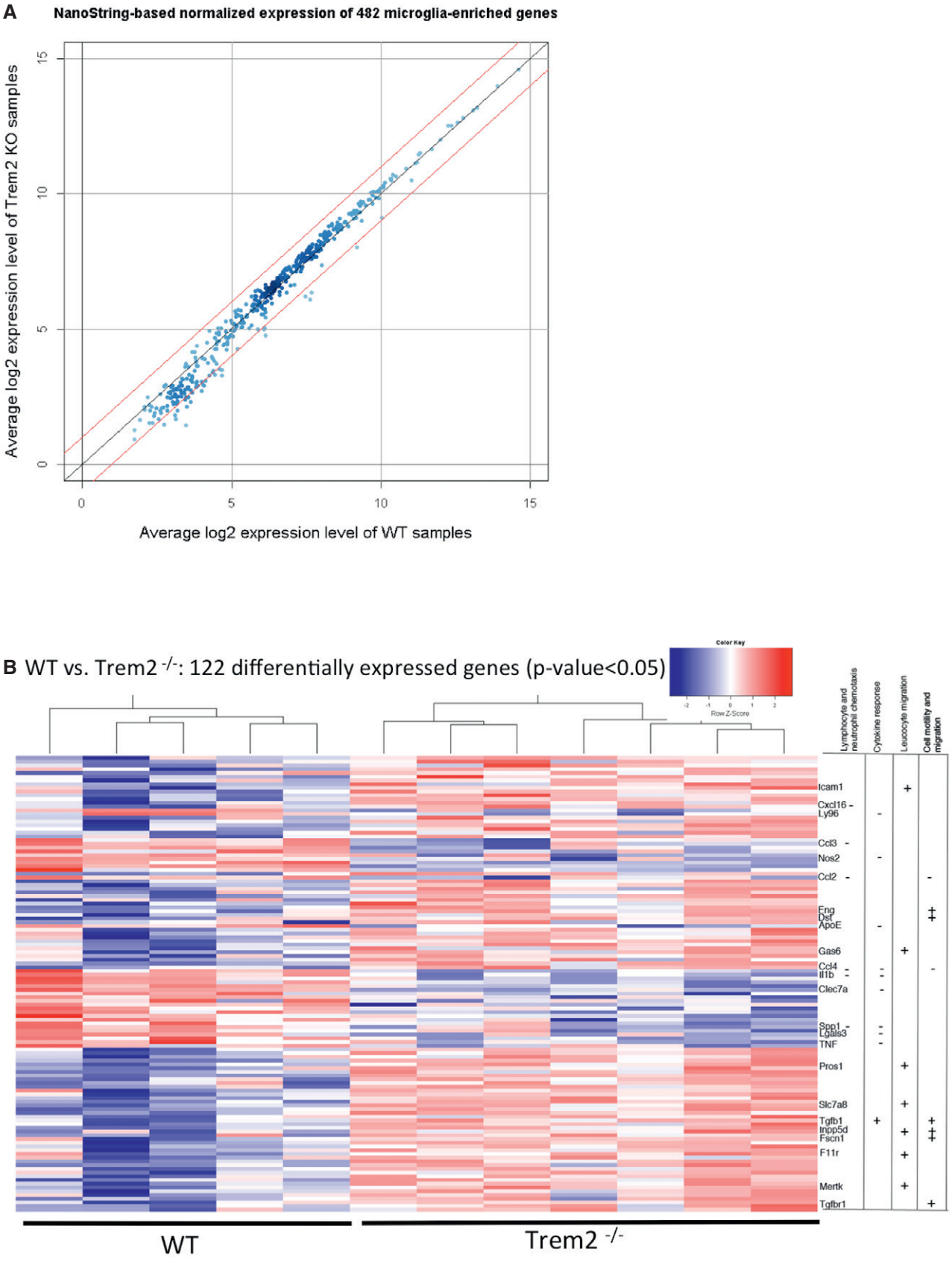

Figure 1.

Table 1. Disturbed regulation of gene clusters involved in chemotaxis and migration.

GO term	Upregulated	Downregulated
Locomotion	INPP5d, CSF3R, DST, P2RY6, PROS1, LIMK1, ABI3, GAB1, SLC7A8, TGFBR1, GAS6, TGFBR2, MERTK, ICAM1, TNFRSF11A, TGFB1, RGMB, SEMA4D, FSCN1	TREM2, CCL2, IL1B, ITGAX, PTPRM, VEGFA, CNTN1, SPP1, CXCL16, APOE, TNF, CSF1, PGRMC1
Cellular component movement	INPP5d, CSF3R, DST, P2RY6, PROS1, ABI1, LIMK1, ABI3, GAB1, SLC7A8, TGFBR1, GAS6, TGFBR2, MERTK, ICAM1, TNFRSF11A, TGFB1, RGMB, SEMA4D, FSCN1	TREM2, CCL2, IL1B, ITGAX, PTPRM, VEGFA, CNTN1, SPP1, CXCL16, APOE, TNF, CSF1, PGRMC1
Cell migration	INPP5d, CSF3R, P2RY6, PROS1, ABI1, LIMK1, ABI3, GAB1, SLC7A8, TGFBR1, GAS6, TGFBR2, MERTK, ICAM1, TNFRSF11A, TGFB1, SEMA4D, FSCN1	CCL2, IL1B, ITGAX, PTPRM, VEGFA, CNTN1, SPP1, CXCL16, APOE, TNF, CSF1
Cell motility	INPP5d, CSF3R, PROS1, SLC7A8, GAS6, MERTK, ICAM1, TNFRSF11A, DST	CCL2, IL1B, ITGAX, VEGFA, SPP1, CXCL16, TNF
Leucocyte migration	INPP5D, CSF3R, PROS1, SLC7A8, GAS6, MERTK, ICAM1, TNFRSF11A	CCL2, IL1B, ITGAX, VEGFA, SPP1, CXCL16, TNF
Response to wounding	INPP5d, FGD2, STAB 1, CSF3R, DST, BASP1, ABI1, TIMP2, LIMK1, INPP4B, TANC2, GAB1, MEF2C, BIN1, NUAK1, TJP1, TGFBR1, GAS6, TGFBR2, MERTK, ICAM1, SPARC, CKB, SALL3, TNFRSF11A, FADS1, TGFB1, USP2, RGMB, SEMA4D	TREM2, CCL2, IL1B, ITGAX, PTPRM, ATF3, VEGFA, CNTN1, SPP1, APOE, TNF, CD83, CSF1, PGRMC1
Neutorophil and lymphocyte chemotaxis	CSF3R	SPP1, IL1B, CXCL16, CCL2

Differentially regulated pathways in Trem2$^{-/-}$ microglia isolated from adult mice. Enrichment of 122 differentially regulated genes in the Gene Ontology (GO) category biological process by the GeneRanker (Genomatix). Significantly overrepresented GO terms with an adjusted *P*-value < 0.05 were deduced. An adjusted *P*-value was estimated from the result of 1,000 simulated null hypothesis queries according to Berriz *et al* [67].

indicate a defect in sensing of certain stimuli and/or a reduced capacity for migration upon a loss of Trem2 function.

Trem2 deficiency decreases migration towards defined chemo-attractants

To specifically investigate the migration capacity towards defined chemo-attractants, we took advantage of a transwell assays [37]. Trem2 is known to act via phosphorylation and activation of Syk [38]. We therefore tested whether inhibition of Syk activation in the N9 microglia cell line [39] might affect their response to chemokines in a transwell assay. Indeed, migration was almost entirely blocked when N9 microglia were pre-incubated with the general tyrosine kinase inhibitor genistein or the Syk-selective inhibitor piceatannol (Fig 3A). Next, we used a CRISPR/CAS9-modified N9 line, which completely lacks Trem2 expression [40] to address whether Trem2 loss of function affects the response to chemotactic stimuli. Using either CCL2 or C5a as chemotactic stimulus, we observed a significantly decreased migration of Trem2-deficient N9 microglia towards both chemotactic stimuli (Fig 3B and C). Importantly, re-expression of mouse Trem2 in the Trem2-deficient cell line fully rescued the chemotactic response towards C5a (Fig 3D and E).

Trem2 deficiency impairs chemotactic migration towards apoptotic neurons *in vivo*

As the innate immune cells of the brain, microglia are the first cells to respond to neuronal damage [16,41]. To test whether the chemotactic deficit that we observed *in vitro* and *ex vivo* can be recapitulated *in vivo*, we measured the ability of microglia to migrate towards apoptotic neurons injected into the brain. Apoptotic neurons are an important hallmark of neurodegeneration, and they are known to release "find-me" signals to attract phagocytes [42,43]. We stereotactically injected Alexa fluor-488-labelled apoptotic neurons in the cortex of adult WT and Trem2$^{-/-}$ mice. Brains were fixed 6 h postinjection and stained with the microglia-specific antibody anti-P2ry12 [15]. WT microglia were attracted to and accumulated around the injected dead neurons as early as 6 h postinjection (Fig 4A). In contrast, we observed a significant reduction in the number of clustered microglia around apoptotic neurons in the absence of Trem2 (Fig 4B; for quantification see Fig 4C). This confirms a critical role of Trem2 in the attraction of microglia towards sites of neuronal injury *in vivo*.

Trem2 deficiency affects outgrowth of microglia processes

Finally, we investigated whether microglia lacking Trem2 are still capable to respond to CNS tissue injury via rapid extension of their processes. To allow *in vivo* imaging of process extension, we crossed WT and Trem2$^{-/-}$ mice with mice expressing green fluorescent protein (GFP) under the control of the Iba1 promoter [44]. In the WT- and Trem2-deficient offspring, we induced a focal CNS damage in the somatosensory cortex using a focussed laser beam [45–47] and acquired time-lapse images of the microglial response using *in vivo* two-photon microscopy (Fig 5A). We then determined the speed of the microglial process extension towards the lesion site (Fig 5A–C). This revealed a significant delay in the response of Trem2$^{-/-}$ microglia close to the injury (immediate area) but not further away (intermediate and distant areas; Fig 5B; for quantification Fig 5C) confirming that the ability of Trem2-deficient microglia to react to nervous system damage is reduced *in vivo*.

Trem2-deficient microglia display a homoeostatic mRNA signature

Systems biological studies revealed a homoeostatic physiological mRNA signature [15], which is distinct from mRNA profiles of microglia in neurodegenerative diseases [48,49]. In mouse models

Published online: May 8, 2017
EMBO reports

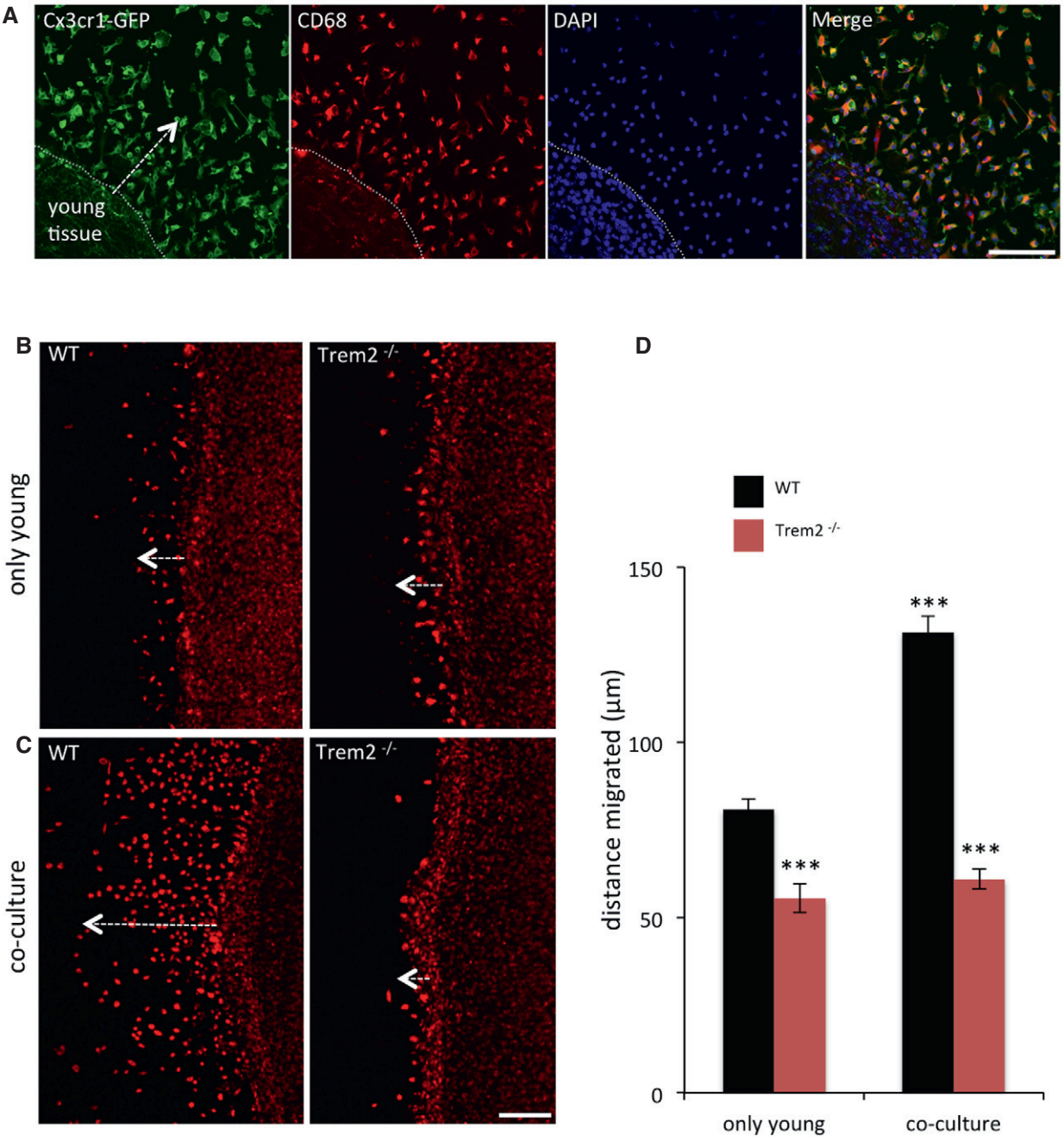

Figure 2. Migration deficits of Trem2$^{-/-}$ microglia in an *ex vivo* assay.

A Cx3cr1-GFP- (green) and CD68 (red)-positive young microglial cells migrate towards old tissue in co-cultures of old APP/PS1 and young Cx3cr1$^{+/GFP}$ brain slices (7 DIV). DAPI (blue) was used to counterstain the nuclei.

B CD68-positive cells migrate out of WT and Trem2$^{-/-}$ brain slices cultured alone (7 DIV). Trem2$^{-/-}$ microglia migrate much shorter distances compared to WT.

C Enhanced migration of CD68-positive microglia in co-cultures of old APP/PS1 and young WT brain slices is abolished in the absence of Trem2.

D Quantitative analysis of the distance migrated by WT or Trem2$^{-/-}$ CD68-positive cells in (B) and (C). N = 4 WT and 4 Trem2$^{-/-}$ mice, from each mouse, two slices were prepared, and on average, 230–550 cells per genotype were analysed. Data are presented as mean ± s.e.m., ***P < 0.001 by using a one-way analysis of variance with Tukey *post hoc* comparison. P-values: WT young only versus Trem2$^{-/-}$ young only: ***P = 0.001; WT young only versus WT co-culture: ***P = 0.001; Trem2$^{-/-}$ young only versus Trem2$^{-/-}$ co-culture: P = 0.8999; WT co-culture versus Trem2$^{-/-}$ co-culture: ***P = 0.001.

Data information: Scale bars, 100 µm. For (A–C), white arrows indicate migration of microglia cells.

for AD and ALS, many genes typically expressed under physiological conditions such as *Csf1r*, *Cx3cr1*, *Tmem119*, *Tgfbr1*, *P2ry12* or *Il10ra* are selectively downregulated [49,50]. Since apparently microglia lacking TREM2 are unable to respond to various types of chemo-attractants and neuronal injury, we asked whether in Trem2$^{-/-}$ microglia the homoeostatic mRNA signature is preserved.

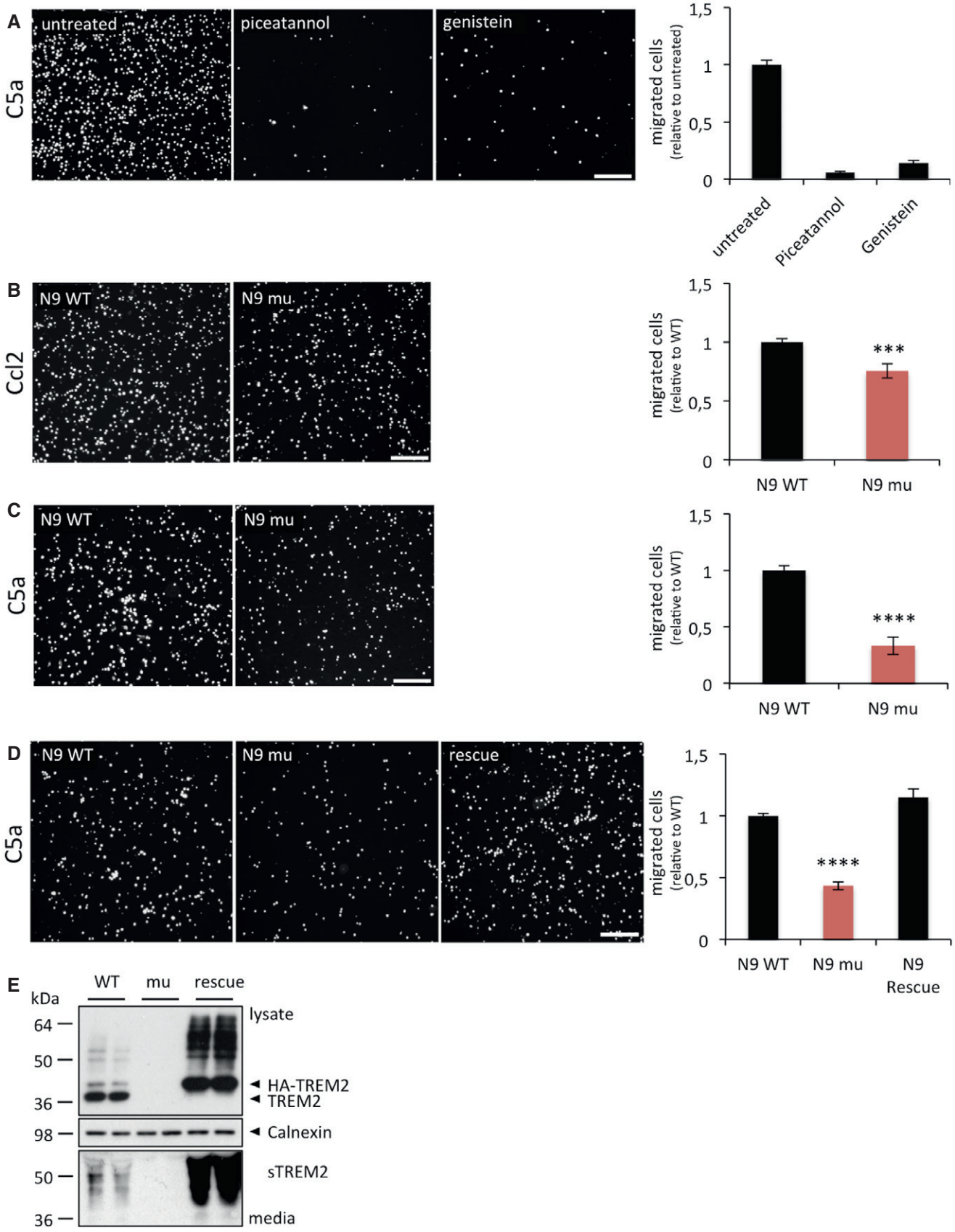

Figure 3.

Figure 3. Migration of N9 microglia cells towards chemotactic stimuli in a transwell assay.

A N9 cell migration in the presence and absence of the general tyrosine kinase inhibitor genistein and the Syk-selective inhibitor piceatannol. $P = 0.00001$, $N = 12$ for each condition.

B Migration capacity of wild-type N9 microglia (WT) or Trem2-deficient N9 microglia (N9 mu) towards 100 ng/ml recombinant mouse Ccl2. $P = 0.00041$, $N = 18$ for WT and $N = 18$ for Trem2$^{-/-}$.

C Migration capacity of wild-type N9 microglia (WT) or Trem2-deficient N9 microglia (N9 mu) towards 25 ng/ml recombinant mouse C5a. $P = 0.00001$, $N = 19$ for WT and $N = 17$ for Trem2$^{-/-}$.

D The migration deficit of Trem2-deficient N9 cells is fully restored upon expression of mouse Trem2. $P = 0.00001$, $N = 6$.

E Western blot analysis of lysates (upper panel) and media (lower panel) from WT, mutant and N9 cells re-expressing TREM2 using the anti-murine TREM2 antibody 5F4 raised against the murine TREM2 extracellular domain. sTREM2, soluble TREM2. Calnexin (middle panel), loading control.

Data information: In panels (A–D), DAPI-stained cells are shown on the left and quantitation is shown on the right side. Values are normalized to WT N9 cells and represent mean ± s.e.m., normalized to the WT N9 mean. *P*-values were determined according to a two-tailed Student's *t*-test. Scale bars, 200 μm.
Source data are available online for this figure.

Microglia were analysed for changes in the expression of selected homoeostatic genes using the above-described NanoString-based chips [15] (Fig 6A). This revealed that expression of homoeostatic genes was not suppressed but rather fully maintained and even slightly but significantly increased (Fig 6B).

Discussion

Microglia are the resident macrophages of the central nervous system and play a pivotal role in synaptic pruning and apoptotic cell clearance during development of the nervous system [51–56]. In the adult brain, microglia are of central importance for brain homoeostasis. Furthermore, in almost all neurodegenerative disorders, microgliosis is a major pathological hallmark although it is not entirely clear whether activated microglia drive or slow disease progression. Increasing evidence for a pathological role of microglia in onset and progression of neurodegenerative diseases is derived from genomewide association studies, which led to the identification of TREM2 and other microglia-related risk genes [7,11]. Certain mutations in *TREM2* inhibit its maturation and transport to the cell surface and result in reduced phagocytosis, lipid sensing and ApoE binding, thus clearly indicating a loss of function [17,19–23]. A loss of function of TREM2 in disease is further supported by null mutations in TREM2 and its binding partner DAP12, which are causative for Nasu–Hakola disease [57]. However, the molecular and cellular mechanisms responsible for dysfunctional microglia in the absence of TREM2 are not well understood. Understanding such consequences will help to unravel the physiological and pathological function of TREM2 and may open new avenues for therapeutic modulation of neurodegenerative disorders. Moreover, systems analyses may shed light on the important question whether

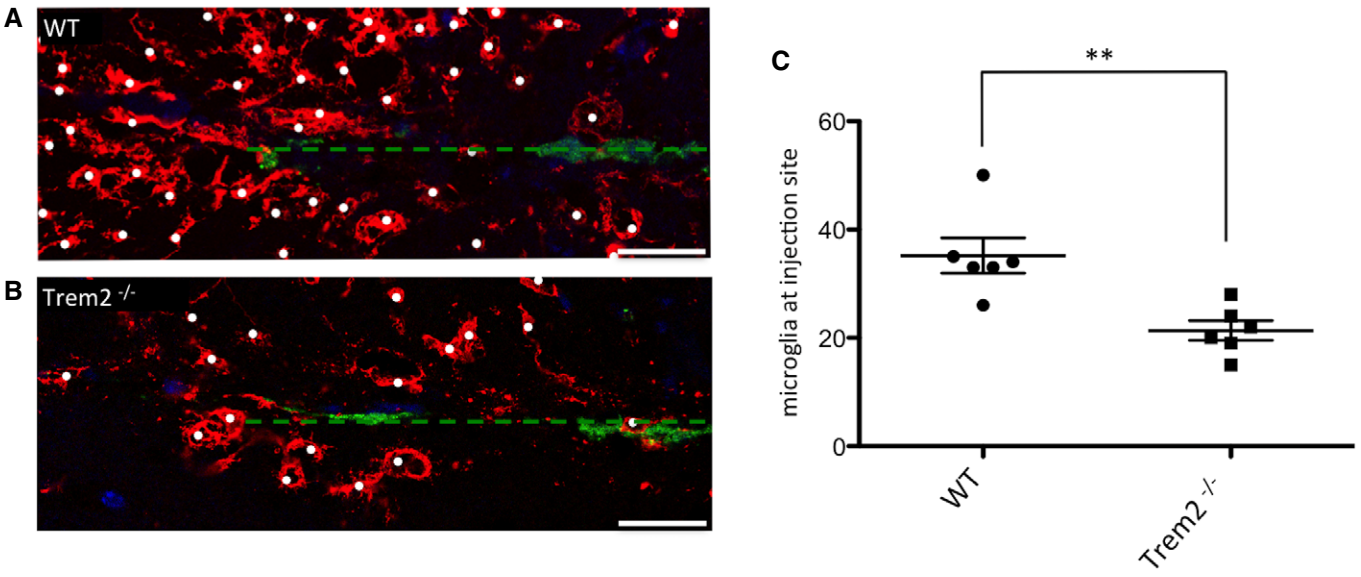

Figure 4. Reduced migration of Trem2-deficient microglia towards apoptotic neurons *in vivo*.

A, B Migration of microglia towards injected Alexa 488-labelled apoptotic neurons (green) in WT (A) and Trem2$^{-/-}$ (B) mouse brains. Microglial cells are visualized with the anti-P2ry12 antibody (red) and nuclei with DAPI (blue). Dashed line indicates injection channel. Scale bar, 25 μm.

C Quantification of the number of microglia (labelled with white dots) clustered around the injection site. $N = 6$ individual mice per genotype. $^{**}P = 0.004$ according to a two-tailed Student's *t*-test. The scatter plot shows data points from individual experiments. Horizontal lines represent mean values, error bars indicate standard deviations.

Source data are available online for this figure.

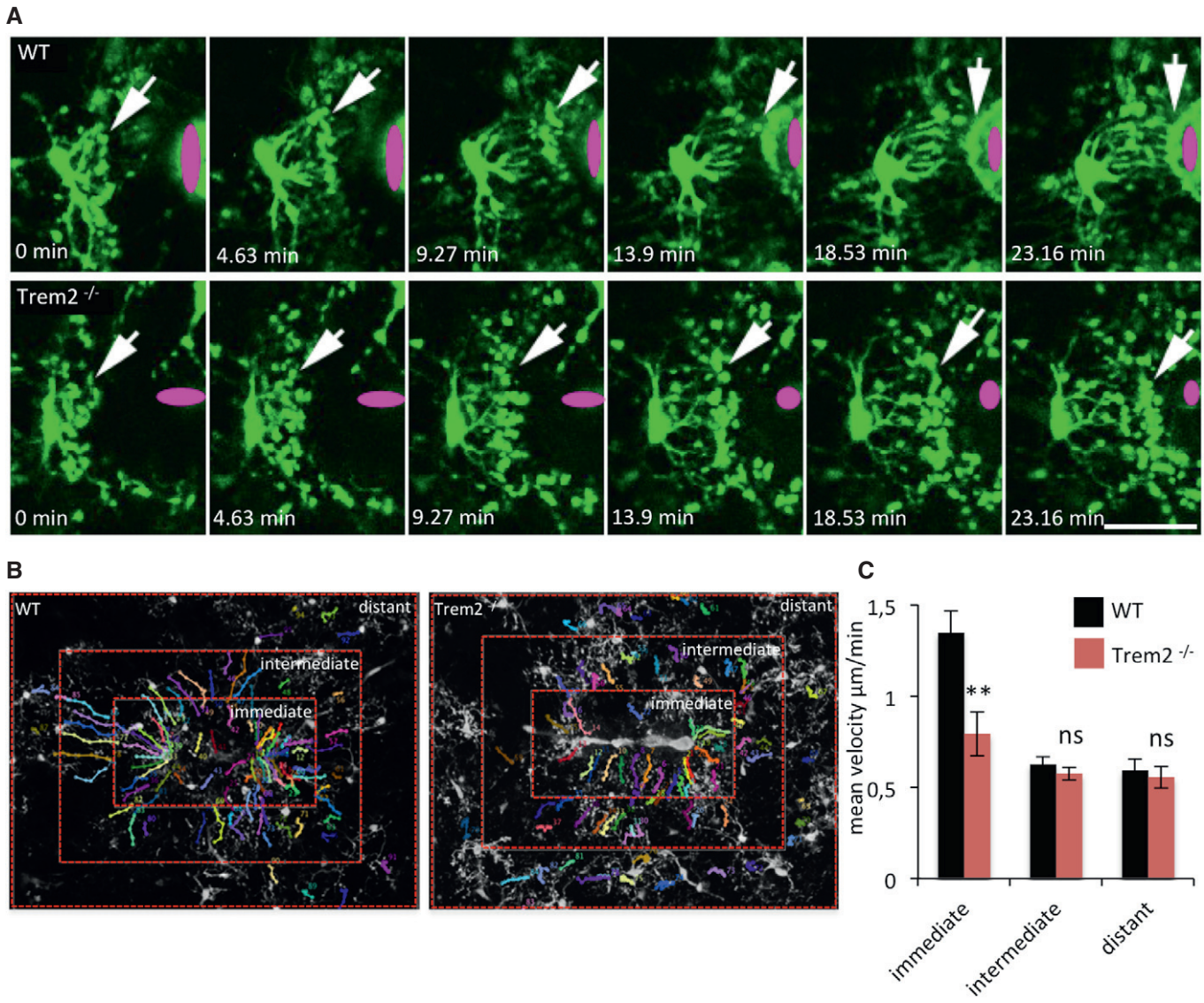

Figure 5. Impaired wound response in Trem2-deficient microglia *in vivo*.

A Early response of Iba1-GFP WT or Trem2$^{-/-}$ microglia towards a laser lesion (indicated in magenta). White arrows point to the microglial processes. Time between each frame is 278 seconds. Scale bar, 25 µm.

B Areas used to quantitate process outgrowth speeds.

C Quantification of the speed of process outgrowth. Data are presented as mean ± s.e.m., $^{**}P$ = 0.0016 according to Mann–Whitney *U*-test (*N* = number of injuries: WT = 13 injuries in five mice; Trem2$^{-/-}$ = 8 injuries in three mice).

Source data are available online for this figure.

microglia prevent or promote disease progression. To obtain insights into Trem2-associated functional pathways, we isolated microglia from brains of WT or Trem2$^{-/-}$ mice using previously characterized highly selective antibodies [15] and compared their homoeostatic mRNA signature using the NanoString technology. We found that in the absence of Trem2, the homoeostatic signature was not suppressed, since many of the characteristic genes found to be expressed under resting conditions were expressed at even slightly higher levels. Interestingly, one of the genes whose expression is even slightly upregulated is *Sall1*. Sall1 acts to maintain microglial identity *in vivo,* and its inactivation leads to the conversion of microglia from resting into an inflammatory state [58]. Thus, failure of Sall1 suppression in the absence of Trem2 may further stabilize a resting state of microglia. Moreover, microglia deficient for Trem2 showed a significant increase in *TGFbr1*. TGFb1 signalling is required for maintaining the unique molecular signature that is characteristic for adult resting microglia *in vivo* [15]. Furthermore, expression of TGFbr1 is downregulated in a mouse model for familial amyotrophic lateral sclerosis (ALS) as well as in human sporadic and familial ALS [48]. Based on these findings, we predict that a loss of function of Trem2 may lock microglia in a resting state and prevents them from being activated. Since several loss-of-function

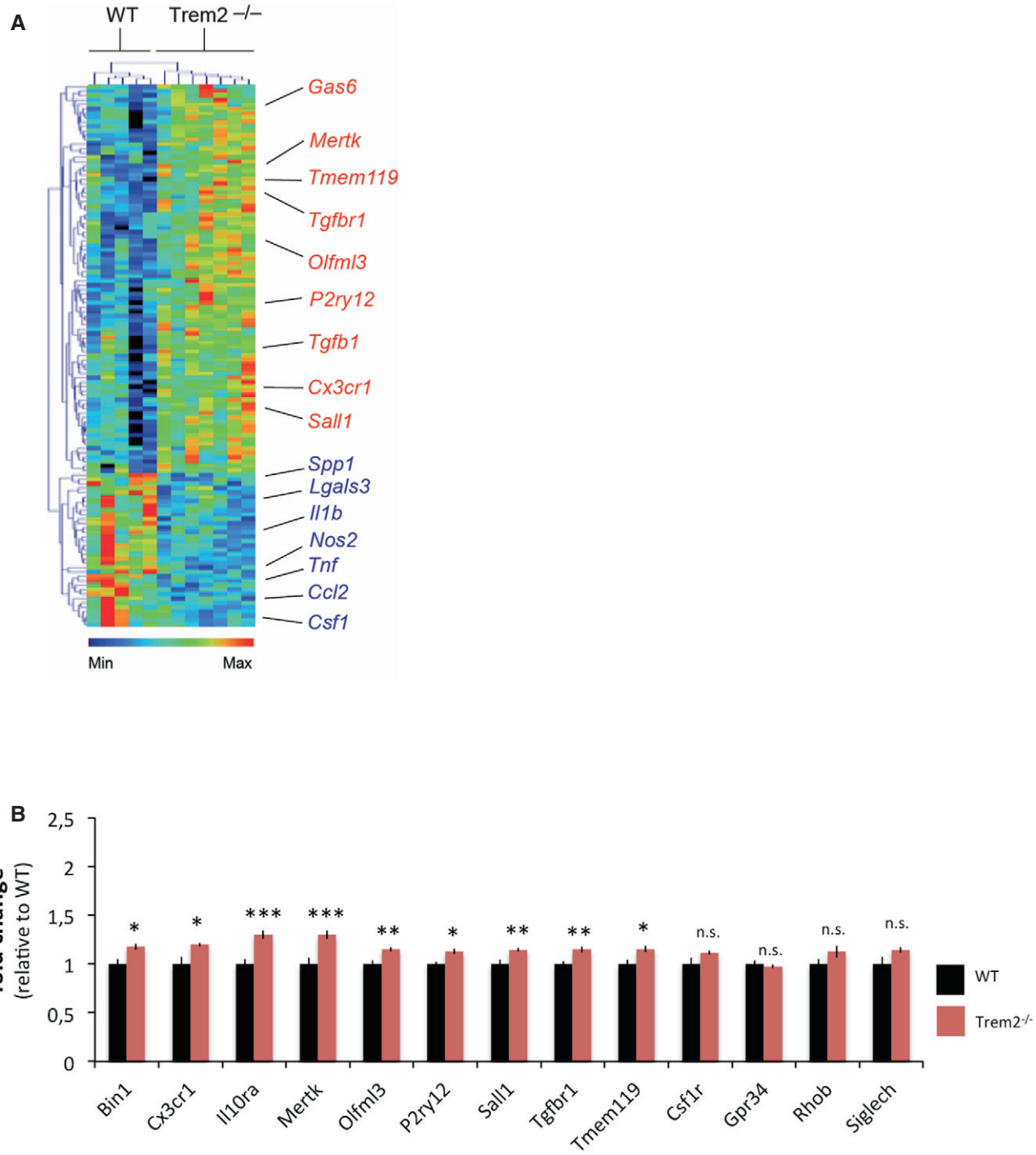

Figure 6. Sustained expression of microglial homoeostatic genes in the absence of Trem2.

A Heat map demonstrating altered expression levels of microglial genes in FACS-sorted microglia from WT and Trem2$^{-/-}$ mice as determined by NanoString analysis. Heat map and hierarchical clustering of microglia were analysed with the MG400 chip. Results were log-transformed, normalized and centred, and populations and genes were clustered by Pearson correlation using MeV v4.6.

B Expression levels of homoeostatic microglial genes in FACS-sorted microglia derived from WT and Trem2$^{-/-}$ mice as determined by NanoString analysis. Bars show levels of mRNA transcripts in the respective models normalized to six independent housekeeping genes. Values indicate mean ± s.e.m. per 100 ng of total RNA. $^{*}P < 0.05$, $^{**}P < 0.01$, $^{***}P < 0.001$ by two-tailed Student's *t*-test. *P*-values: Trem2$^{-/-}$ versus WT, *Bin1* $^{*}P = 0.012$, *Cx3cr1* $^{*}P = 0.012$, *Il10ra* $^{***}P = 0.001$, *Mertk* $^{***}P = 0.002$, *Olfml3* $^{**}P = 0.005$, *P2ry12* $^{*}P = 0.011$, *Sall1* $^{**}P = 0.005$, *Tgfbr1* $^{**}P = 0.006$, *Tmem119* $^{*}P = 0.02$, *Csf1r* $P = 0.081$, *Gpr34* $P = 0.505$, *Rhob* $P = 0.164$, *Siglech* $P = 0.062$. Data were generated from the same samples as in Fig 1; WT $N = 5$, Trem2$^{-/-}$ $N = 7$.

Source data are available online for this figure.

variants of TREM2 are associated with neurodegenerative conditions in humans, this also suggests that a normal function of TREM2 may be a protective response, which could be involved in slowing disease progression. This is in line with the finding that sTREM2 increases during healthy ageing, which may reflect an increase of TREM2 function via enhanced TREM2 levels on the cell surface [24,27,59]. Moreover, sTREM2 was even further enhanced in asymptomatic stages of patients of the DIAN cohort [27] and in patients with very mild cognitive impairment in a sporadic AD cohort [24]. The increase of sTREM2 was also associated with increased CSF levels of total tau and phosphorylated tau suggesting that TREM2 expression and function may be stimulated by injured neurons and that the failure to appropriately respond to such injuries may be associated with accelerated disease progression. Moreover, failure of $Trem2^{-/-}$ microglia to appropriately respond to chemotactic stimuli, which we confirmed by a wide variety of independent assays, is also in line with a protective function of WT TREM2. This is also consistent with the observation that microglia fail to cluster around amyloid plaques in the absence of Trem2 [31,60,61]. Moreover, treatment of microglia with TGFb1 attenuates microglial migration towards aggregated amyloid β-peptide by dysregulating chemotactic genes [62]. This finding is consistent with the upregulation of Tgfbr1 in the absence of Trem2 and our prediction that microglia are locked in a resting state when Trem2 is absent or dysfunctional due to disease-associated sequence variants. However, we performed all phenotypic analyses in the complete absence of Trem2. It therefore remains to be shown if single AD-associated point mutations expressed at the endogenous level would also result in similar loss-of-function phenotypes.

Materials and Methods

Animal experiments and licence

The $Cx3cr1^{GFP/GFP}$ reporter line [36] was obtained from the Jackson Laboratory and bred with C57BL/6J WT to obtain $CX_3CR1^{+/GFP}$ mice. Iba1-GFP mice are described in [44].

Hemizygous APPPS1 mice overexpressing human $APP_{KM670/671NL}$ and $PS1_{L166P}$ under the control of the Thy-1 promoter (line 21) were kindly provided by Mathias Jucker (Hertie-Institute for Clinical Brain Research, University of Tübingen and DZNE-Tübingen) [35] and bred in a C57BL/6J background. Trem2 KO mice were kindly provided by Marco Colonna (Washington University, School of Medicine) [63].

All animal experiments were performed in accordance with local animal handling laws.

Microglia isolation

For microglia isolation, adult male mice (3.5–4 months) were sacrificed by CO_2 followed by a cervical dislocation. Brains were homogenized in HBSS by mechanical dissociation; cell suspensions were filtered through a 100-μm cell strainer and separated in a 40–70% Percoll gradient (GE Healthcare). Mononuclear cells were collected from the interface and washed once with blocking buffer (0.2% bovine serum albumin in HBSS). These cells were then stained sequentially with monoclonal FCRLS [15] and CD11b antibodies (BD Biosciences) and sorted using a Becton Dickinson FACSARIA II cell sorter. Total RNA was isolated and gene expression profiling was performed using the NanoString technology as described [15,48].

Data normalization and analysis

Gene expression levels in each sample were normalized against the geometric mean of six housekeeping genes including *Cltc*, *Gapdh*, *Gusb*, *Hprt1*, *Pgk1* and *Tubb5*. Based on the normalized gene expression levels of NanoString-based chips, a two-tailed Student's *t*-test assuming equal variance was applied to each gene to compare the difference between the $Trem2^{-/-}$ group consisting of seven mice and the WT group consisting of five mice. A false discovery rate (FDR) for each *P*-value was calculated according to Benjamini and Hochberg [64] by using p.adjust (method = "BH") in R statistical software (www.r-project.org). Entrez Gene IDs of genes which show $P < 0.05$ were then imported into the GeneRanker program from Genomatix (Munich, Germany) by using the database versions ElDorado 12-2013 and Genomatix Literature Mining 11-2013 to perform an enrichment analysis on the Gene Ontology (GO) functional categories.

Organotypic slice cultures and *ex vivo* migration assay

Organotypic slice cultures were performed and immunostained as described by Daria *et al* [34]. In the co-culture paradigm, two slices of young P5 tissue (WT, $Trem2^{-/-}$ or $Cx3cr1^{+/GFP}$) were plated together with two slices of old (10–12 months) APPPS1 tissue. The migration distance was measured 7 days after the culturing *ex vivo*. The migration distance was measured using Fiji [65] by drawing a line between the migrated cell and the slice culture border. In total, up to 550 (WT) and 400 ($Trem2^{-/-}$) cells were analysed from eight slices (four mice per genotype).

Cell migration in transwell assays

N9 cells [39] and the CRISPR/CAS9-generated TREM2 mutant cell line were described before [40]. Re-expression of WT TREM2 in TREM2 knockout cells was achieved by transfecting N-terminal tagged full-length murine Trem2 in a pcDNA3.1 vector. Twenty-four hours after transfection, cells were selected with 200 μg/ml Zeocin for 2 weeks. Single-cell clones were cultured in media containing 100 μg/ml Zeocin medium, followed by Western blot analysis.

N9 cell migration towards 100 ng/ml of recombinant murine JE/MCP-1 (CCL2); Peprotech) or 20 ng/ml of recombinant murine complement component C5a (R&D Systems) was tested in transwell assays (COSTAR 24-well plate with inserts, 8-μm pore, Corning, NY). For Syk inhibition, cells were incubated overnight in 50 μM genistein (Sigma) or piceatannol (Tocris).

For the transwell assays, 600 μl media (DMEM complemented with GlutaMAX™ (Life Technologies)) together with the attractant were added to the bottom well and 5×10^5 cells were cultured in 100 μl media in the top well. Migration was assayed for 2 h at 37°C and 5% CO_2. Subsequently, inserts were removed and washed three times with PBS. Cells were then fixed with 4% PFA for 15 min, followed by permeabilization with PBS containing 0.2% Triton X-100. Stationary cells were removed from the top, and cells that migrated through the filter to the lower side of the transwell filter

were stained with DAPI and images were taken. Two fields for each well were selected for imaging, and the migrated cells were quantified using Fiji software.

Stereotactic injection of apoptotic neurons

To induce apoptosis, neurons were carefully detached from the plate surface by repeated washes with PBS. Neurons were irradiated with UV light (302 nm) with an intensity of 6 × 15 W for 15 min. Cells were harvested by centrifugation, and the pellet processed for downstream applications. Neurons were incubated for 15 min at 37°C with 2 μl of the labelling dye (Alexa488 5-SDP Ester or Alexa405 5-SDP, Life Technologies). To block and capture residual dye, cells were resuspended in 1 ml FBS and washed twice with PBS. Total apoptotic cell number was determined using trypan blue staining and resuspended at a density of ~100,000 cells per 2 μl for stereotactic injection. Mice were anesthetized by i.p. injection of a mixture of ketamine (100 mg/kg), xylazine (10 mg/kg) and acepromazine (3 mg/kg); 2 μl of Alexa488-labelled apoptotic neurons or saline solution was distributed intrahippocampal and intracortical bilaterally (Y: ± 1.5 mm; X: −2 mm; Z: −2 mm and −1 mm) using stereotaxic equipment (Harvard Apparatus). After recovery from surgery, animals were returned to their home cages. Postsurgery (16 h), mice were euthanized by CO_2 inhalation and perfused for subsequent experiments.

For histological analyses of microglia migration towards Alexa 488-labelled and injected apoptotic neurons, brains were perfused with ice-cold HBSS, fixed in 4% buffered formalin and subsequently embedded in paraffin. Stepwise sections were taken and paraffin sections (3 μm) were collected when the injection channel was clearly visible. After dewaxing, antigen retrieval was performed by boiling the sections for 30 min in 10 mM citrate buffer, pH 6.0. Sections were washed, permeabilized with 0.2% Triton X-100 (Roche) in TBS and blocked for 1 h (Protein-Free T20 (TBS) Blocking buffer #37071 Thermo Fischer). The microglia-specific antibody P2ry12 [15] was incubated in blocking buffer overnight at 4°C with constant shaking, followed by intensive washing and incubation with an Alexa-555-coupled anti-rabbit secondary antibody for 1 h. Sections were washed again and mounted with DAPI-Fluoromount-G (SouthernBiotech). Data acquisition was performed using a Leica Sp5 confocal microscope and Leica application suite software (LAS-AF-lite).

In vivo imaging of process outgrowth

To image the microglia process outgrowth upon laser lesion in controlled conditions, cranial windows were implanted over the somato-sensory cortex of Iba1-GFP WT and Iba1-GFP/Trem2$^{-/-}$ mice 14 days prior to imaging and laser lesion induction (for details, see [66]). On the day of imaging, animals were anaesthetized using a mixture of medetomidine, midazolom and fentanyl (MMF; 150–200 μl/kg) 30 min prior to the start of the experiment. Laser lesions of ~150 μm length were performed 30 μm below the cortical surface, and the microglia response was recorded every 5 min for 90 min over an area of 250,000 μm^2 from the cortical surface to 70 μm depth.

The extension of individual processes was tracked using the mTrackJ plug-in of the Fiji software [65] package. Briefly, cells located in a field of 20,000, 60,000 or 120,000 μm^2 (immediate, intermediate and distant areas, respectively) around the injury were selected for manual tracking. The data were exported to Excel for analysis, and the mean velocity of the extension was calculated for each microglia process. More than 200 outgrowing tracks from a minimum of three independent experiments were analysed for each experimental condition manner. Data analysis was confirmed by independent co-workers in a blinded manner.

MG400 microglia nCounter chip design

The MG400 chip was designed using the quantitative NanoString nCounter platform. Selection of genes is based on analyses that identified genes and proteins, which are specifically or highly expressed in adult mouse microglia [15].

Expanded View for this article is available online.

Acknowledgements
This work was supported by the Deutsche Forschungsgemeinschaft (DFG) within the framework of the Munich Cluster for Systems Neurology (EXC 1010 SyNergy), the European Research Council under the European Union's Seventh Framework Program (FP7/2007–2013)/ERC Grant Agreement No. 321366-Amyloid, the general legacy of Mrs. Ammer, the MetLife award and the Cure Alzheimer's Fund. We thank Kristin Hartmann for technical assistance. T.M was further supported by the Center for Integrated Protein Science Munich (CIPSM, EXC 114), SFB 870 and Research Grants Mi 694/4-1(SPP1710)/7-1/8-1. Further support came from the European Research Council under the European Union's Seventh Framework Program (FP/2007-2013; ERC Grant Agreement n. 616791) and the Hans-and-Ilse-Breuer Foundation. This work was supported by the German Science Foundation Collaborative Research Centre (CRC) 870. In addition, this work was funded in part by the Helmholtz Portfolio Theme "Supercomputing and Modeling for the Human Brain" (SMHB). O.B. is supported by NIH-NINDS (1R01NS088137), NIA (1R01AG051812), National Multiple Sclerosis Society (5092A1), Amyotrophic Lateral Sclerosis Association (ALSA2087) and the Nancy Davis Foundation. We thank Jochen Herms for providing Iba1-GFP mice.

Author contributions
CH and FM conceived the study and analysed the results. CH wrote the manuscript with help from all co-authors. FM carried out the transwell assays, isolated microglia, prepared RNA samples, performed the *ex vivo*, *in vitro* and *in vivo* data analyses. GK helped with the microglia isolation and interpretation of the results. AD and ST conducted the *ex vivo* culturing and immunofluorescence analysis. GW generated the genetically modified N9 cells. NS, TM and MK conceived and performed the two-photon imaging experiments. DT and WW performed the pathway analysis. AC helped with the transwell assays and generation of the N9 mutant cell line. BB provided technical assistance. SB assisted with cell sorting. OB, CM and SK conducted the NanoString analysis and injection of apoptotic neurons.

Conflict of interest
C.H. is an advisor of F. Hoffmann-La Roche. All other authors declare that they have no conflict of interest.

References

1. Aguzzi A, Haass C (2003) Games played by rogue proteins in prion disorders and Alzheimer's disease. *Science* 302: 814 – 818

2. Haass C, Selkoe DJ (2007) Soluble protein oligomers in neurodegeneration: lessons from the Alzheimer's amyloid beta-peptide. *Nat Rev Mol Cell Biol* 8: 101 – 112
3. Jucker M, Walker LC (2013) Self-propagation of pathogenic protein aggregates in neurodegenerative diseases. *Nature* 501: 45 – 51
4. Heneka MT, Carson MJ, El Khoury J, Landreth GE, Brosseron F, Feinstein DL, Jacobs AH, Wyss-Coray T, Vitorica J, Ransohoff RM *et al* (2015) Neuroinflammation in Alzheimer's disease. *Lancet Neurol* 14: 388 – 405
5. Borroni B, Ferrari F, Galimberti D, Nacmias B, Barone C, Bagnoli S, Fenoglio C, Piaceri I, Archetti S, Bonvicini C *et al* (2014) Heterozygous TREM2 mutations in frontotemporal dementia. *Neurobiol Aging* 35: 934.e7 – 934.e10
6. Cady J, Koval ED, Benitez BA, Zaidman C, Jockel-Balsarotti J, Allred P, Baloh RH, Ravits J, Simpson E, Appel SH *et al* (2014) TREM2 variant p. R47H as a risk factor for sporadic amyotrophic lateral sclerosis. *JAMA Neurol* 71: 449 – 453
7. Guerreiro R, Bilgic B, Guven G, Bras J, Rohrer J, Lohmann E, Hanagasi H, Gurvit H, Emre M (2013) Novel compound heterozygous mutation in TREM2 found in a Turkish frontotemporal dementia-like family. *Neurobiol Aging* 34: 2890.e1 – 2890.e5
8. Guerreiro R, Hardy J (2013) TREM2 and neurodegenerative disease. *N Engl J Med* 369: 1569 – 1570
9. Guerreiro R, Wojtas A, Bras J, Carrasquillo M, Rogaeva E, Majounie E, Cruchaga C, Sassi C, Kauwe JS, Younkin S *et al* (2013) TREM2 variants in Alzheimer's disease. *N Engl J Med* 368: 117 – 127
10. Guerreiro RJ, Lohmann E, Bras JM, Gibbs JR, Rohrer JD, Gurunlian N, Dursun B, Bilgic B, Hanagasi H, Gurvit H *et al* (2013) Using exome sequencing to reveal mutations in TREM2 presenting as a frontotemporal dementia-like syndrome without bone involvement. *JAMA Neurol* 70: 78 – 84
11. Jonsson T, Stefansson H, Steinberg S, Jonsdottir I, Jonsson PV, Snaedal J, Bjornsson S, Huttenlocher J, Levey AI, Lah JJ *et al* (2013) Variant of TREM2 associated with the risk of Alzheimer's disease. *N Engl J Med* 368: 107 – 116
12. Rayaprolu S, Mullen B, Baker M, Lynch T, Finger E, Seeley WW, Hatanpaa KJ, Lomen-Hoerth C, Kertesz A, Bigio EH *et al* (2013) TREM2 in neurodegeneration: evidence for association of the p. R47H variant with frontotemporal dementia and Parkinson's disease. *Mol Neurodegener* 8: 19
13. Klunemann HH, Ridha BH, Magy L, Wherrett JR, Hemelsoet DM, Keen RW, De Bleecker JL, Rossor MN, Marienhagen J, Klein HE *et al* (2005) The genetic causes of basal ganglia calcification, dementia, and bone cysts: DAP12 and TREM2. *Neurology* 64: 1502 – 1507
14. Colonna M, Wang Y (2016) TREM2 variants: new keys to decipher Alzheimer disease pathogenesis. *Nat Rev Neurosci* 17: 201 – 207
15. Butovsky O, Jedrychowski MP, Moore CS, Cialic R, Lanser AJ, Gabriely G, Koeglsperger T, Dake B, Wu PM, Doykan CE *et al* (2014) Identification of a unique TGF-beta-dependent molecular and functional signature in microglia. *Nat Neurosci* 17: 131 – 143
16. Ransohoff RM (2016) A polarizing question: do M1 and M2 microglia exist? *Nat Neurosci* 19: 987 – 991
17. Kleinberger G, Yamanishi Y, Suarez-Calvet M, Czirr E, Lohmann E, Cuyvers E, Struyfs H, Pettkus N, Wenninger-Weinzierl A, Mazaheri F *et al* (2014) TREM2 mutations implicated in neurodegeneration impair cell surface transport and phagocytosis. *Sci Transl Med* 6: 243ra86
18. Wunderlich P, Glebov K, Kemmerling N, Tien NT, Neumann H, Walter J (2013) Sequential proteolytic processing of the triggering receptor expressed on myeloid cells-2 (TREM2) protein by ectodomain shedding and gamma-secretase-dependent intramembranous cleavage. *J Biol Chem* 288: 33027 – 33036
19. Colonna M (2003) TREMs in the immune system and beyond. *Nat Rev Immunol* 3: 445 – 453
20. Sieber MW, Jaenisch N, Brehm M, Guenther M, Linnartz-Gerlach B, Neumann H, Witte OW, Frahm C (2013) Attenuated inflammatory response in triggering receptor expressed on myeloid cells 2 (TREM2) knock-out mice following stroke. *PLoS ONE* 8: e52982
21. Atagi Y, Liu CC, Painter MM, Chen XF, Verbeeck C, Zheng H, Li X, Rademakers R, Kang SS, Xu H *et al* (2015) Apolipoprotein E is a ligand for triggering receptor expressed on myeloid cells 2 (TREM2). *J Biol Chem* 290: 26043 – 26050
22. Yeh Felix L, Wang Y, Tom I, Gonzalez Lino C, Sheng M (2016) TREM2 binds to apolipoproteins, including APOE and CLU/APOJ, and thereby facilitates uptake of amyloid-beta by microglia. *Neuron* 91: 328 – 340
23. Bailey CC, DeVaux LB, Farzan M (2015) The triggering receptor expressed on myeloid cells 2 binds apolipoprotein E. *J Biol Chem* 290: 26033 – 26042
24. Suarez-Calvet M, Kleinberger G, Araque Caballero MA, Brendel M, Rominger A, Alcolea D, Fortea J, Lleo A, Blesa R, Gispert JD *et al* (2016) sTREM2 cerebrospinal fluid levels are a potential biomarker for microglia activity in early-stage Alzheimer's disease and associate with neuronal injury markers. *EMBO Mol Med* 8: 466 – 476
25. Piccio L, Deming Y, Del-Aguila JL, Ghezzi L, Holtzman DM, Fagan AM, Fenoglio C, Galimberti D, Borroni B, Cruchaga C (2016) Cerebrospinal fluid soluble TREM2 is higher in Alzheimer disease and associated with mutation status. *Acta Neuropathol* 131: 925 – 933
26. Heslegrave A, Heywood W, Paterson R, Magdalinou N, Svensson J, Johansson P, Ohrfelt A, Blennow K, Hardy J, Schott J *et al* (2016) Increased cerebrospinal fluid soluble TREM2 concentration in Alzheimer's disease. *Mol Neurodegener* 11: 3
27. Suarez-Calvet M, Araque Caballero MA, Kleinberger G, Bateman RJ, Fagan AM, Morris JC, Levin J, Danek A, Ewers M, Haass C *et al* (2016) Early changes in CSF sTREM2 in dominantly inherited Alzheimer's disease occur after amyloid deposition and neuronal injury. *Sci Transl Med* 8: 369ra178
28. Ulrich JD, Finn MB, Wang Y, Shen A, Mahan TE, Jiang H, Stewart FR, Piccio L, Colonna M, Holtzman DM (2014) Altered microglial response to Abeta plaques in APPPS1-21 mice heterozygous for TREM2. *Mol Neurodegener* 9: 20
29. Wang Y, Ulland TK, Ulrich JD, Song W, Tzaferis JA, Hole JT, Yuan P, Mahan TE, Shi Y, Gilfillan S *et al* (2016) TREM2-mediated early microglial response limits diffusion and toxicity of amyloid plaques. *J Exp Med* 213: 667 – 675
30. Yuan P, Condello C, Keene CD, Wang Y, Bird TD, Paul SM, Luo W, Colonna M, Baddeley D, Grutzendler J (2016) TREM2 haplodeficiency in mice and humans impairs the microglia barrier function leading to decreased amyloid compaction and severe axonal dystrophy. *Neuron* 90: 724 – 739
31. Jay TR, Miller CM, Cheng PJ, Graham LC, Bemiller S, Broihier ML, Xu G, Margevicius D, Karlo JC, Sousa GL *et al* (2015) TREM2 deficiency eliminates TREM2+ inflammatory macrophages and ameliorates pathology in Alzheimer's disease mouse models. *J Exp Med* 212: 287 – 295
32. Ma J, Zhou Y, Xu J, Liu X, Wang Y, Deng Y, Wang G, Xu W, Ren R, Liu X *et al* (2014) Association study of TREM2 polymorphism rs75932628 with late-onset Alzheimer's disease in Chinese Han population. *Neurol Res* 36: 894 – 896

33. Zhang WQ, Huang SH, Huang X, Li JH, Ye P, Xu J, Zheng PZ, Shen HY, Huang JR (2016) Regulation of human mesenchymal stem cell differentiation by TREM-2. *Hum Immunol* 77: 476 – 482
34. Daria A, Colombo A, Llovera G, Hampel H, Willem M, Liesz A, Haass C, Tahirovic S (2016) Young microglia restore amyloid plaque clearance of aged microglia. *EMBO J* 36: 583 – 603
35. Radde R, Bolmont T, Kaeser SA, Coomaraswamy J, Lindau D, Stoltze L, Calhoun ME, Jaggi F, Wolburg H, Gengler S *et al* (2006) Abeta42-driven cerebral amyloidosis in transgenic mice reveals early and robust pathology. *EMBO Rep* 7: 940 – 946
36. Jung S, Aliberti J, Graemmel P, Sunshine MJ, Kreutzberg GW, Sher A, Littman DR (2000) Analysis of fractalkine receptor CX(3)CR1 function by targeted deletion and green fluorescent protein reporter gene insertion. *Mol Cell Biol* 20: 4106 – 4114
37. Badie B, Schartner J, Klaver J, Vorpahl J (1999) *In vitro* modulation of microglia motility by glioma cells is mediated by hepatocyte growth factor/scatter factor. *Neurosurgery* 44: 1077 – 1082; discussion 1082-3
38. Paradowska-Gorycka A, Jurkowska M (2013) Structure, expression pattern and biological activity of molecular complex TREM-2/DAP12. *Hum Immunol* 74: 730 – 737
39. Ferrari D, Villalba M, Chiozzi P, Falzoni S, Ricciardi-Castagnoli P, Di Virgilio F (1996) Mouse microglial cells express a plasma membrane pore gated by extracellular ATP. *J Immunol* 156: 1531 – 1539
40. Xiang X, Werner G, Bohrmann B, Liesz A, Mazaheri F, Capell A, Feederle R, Knuesel I, Kleinberger G, Haass C (2016) TREM2 deficiency reduces the efficacy of immunotherapeutic amyloid clearance. *EMBO Mol Med* 8: 992 – 1004
41. Kettenmann H, Hanisch UK, Noda M, Verkhratsky A (2011) Physiology of microglia. *Physiol Rev* 91: 461 – 553
42. Medina CB, Ravichandran KS (2016) Do not let death do us part: "find-me" signals in communication between dying cells and the phagocytes. *Cell Death Differ* 23: 979 – 989
43. Ravichandran KS, Lorenz U (2007) Engulfment of apoptotic cells: signals for a good meal. *Nat Rev Immunol* 7: 964 – 974
44. Hirasawa T, Ohsawa K, Imai Y, Ondo Y, Akazawa C, Uchino S, Kohsaka S (2005) Visualization of microglia in living tissues using Iba1-EGFP transgenic mice. *J Neurosci Res* 81: 357 – 362
45. Nimmerjahn A, Kirchhoff F, Helmchen F (2005) Resting microglial cells are highly dynamic surveillants of brain parenchyma *in vivo*. *Science* 308: 1314 – 1318
46. Davalos D, Grutzendler J, Yang G, Kim JV, Zuo Y, Jung S, Littman DR, Dustin ML, Gan WB (2005) ATP mediates rapid microglial response to local brain injury *in vivo*. *Nat Neurosci* 8: 752 – 758
47. Fourgeaud L, Traves PG, Tufail Y, Leal-Bailey H, Lew ED, Burrola PG, Callaway P, Zagorska A, Rothlin CV, Nimmerjahn A *et al* (2016) TAM receptors regulate multiple features of microglial physiology. *Nature* 532: 240 – 244
48. Butovsky O, Jedrychowski MP, Cialic R, Krasemann S, Murugaiyan G, Fanek Z, Greco DJ, Wu PM, Doykan CE, Kiner O *et al* (2015) Targeting miR-155 restores abnormal microglia and attenuates disease in SOD1 mice. *Ann Neurol* 77: 75 – 99
49. Holtman IR, Raj DD, Miller JA, Schaafsma W, Yin Z, Brouwer N, Wes PD, Moller T, Orre M, Kamphuis W *et al* (2015) Induction of a common microglia gene expression signature by aging and neurodegenerative conditions: a co-expression meta-analysis. *Acta Neuropathol Commun* 3: 31
50. Chiu IM, Morimoto ET, Goodarzi H, Liao JT, O'Keeffe S, Phatnani HP, Muratet M, Carroll MC, Levy S, Tavazoie S *et al* (2013) A neurodegeneration-specific gene-expression signature of acutely isolated microglia from an amyotrophic lateral sclerosis mouse model. *Cell Rep* 4: 385 – 401
51. Sierra A, Encinas JM, Deudero JJ, Chancey JH, Enikolopov G, Overstreet-Wadiche LS, Tsirka SE, Maletic-Savatic M (2010) Microglia shape adult hippocampal neurogenesis through apoptosis-coupled phagocytosis. *Cell Stem Cell* 7: 483 – 495
52. Schafer Dorothy P, Lehrman Emily K, Kautzman Amanda G, Koyama R, Mardinly Alan R, Yamasaki R, Ransohoff Richard M, Greenberg Michael E, Barres Ben A, Stevens B (2012) Microglia sculpt postnatal neural circuits in an activity and complement-dependent manner. *Neuron* 74: 691 – 705
53. Schafer DP, Lehrman EK, Stevens B (2013) The "quad-partite" synapse: microglia-synapse interactions in the developing and mature CNS. *Glia* 61: 24 – 36
54. Stevens B, Allen NJ, Vazquez LE, Howell GR, Christopherson KS, Nouri N, Micheva KD, Mehalow AK, Huberman AD, Stafford B *et al* (2007) The classical complement cascade mediates CNS synapse elimination. *Cell* 131: 1164 – 1178
55. Mazaheri F, Breus O, Durdu S, Haas P, Wittbrodt J, Gilmour D, Peri F (2014) Distinct roles for BAI1 and TIM-4 in the engulfment of dying neurons by microglia. *Nat Commun* 5: 4046
56. Paolicelli RC, Bolasco G, Pagani F, Maggi L, Scianni M, Panzanelli P, Giustetto M, Ferreira TA, Guiducci E, Dumas L *et al* (2011) Synaptic pruning by microglia is necessary for normal brain development. *Science* 333: 1456 – 1458
57. Paloneva J, Kestila M, Wu J, Salminen A, Bohling T, Ruotsalainen V, Hakola P, Bakker AB, Phillips JH, Pekkarinen P *et al* (2000) Loss-of-function mutations in TYROBP (DAP12) result in a presenile dementia with bone cysts. *Nat Genet* 25: 357 – 361
58. Buttgereit A, Lelios I, Yu X, Vrohlings M, Krakoski NR, Gautier EL, Nishinakamura R, Becher B, Greter M (2016) Sall1 is a transcriptional regulator defining microglia identity and function. *Nat Immunol* 17: 1397 – 1406
59. Henjum K, Almdahl IS, Arskog V, Minthon L, Hansson O, Fladby T, Nilsson LN (2016) Cerebrospinal fluid soluble TREM2 in aging and Alzheimer's disease. *Alzheimers Res Ther* 8: 17
60. Ulrich JD, Holtzman DM (2016) TREM2 function in Alzheimer's Disease and neurodegeneration. *ACS Chem Neurosci* 7: 420 – 427
61. Wang Y, Cella M, Mallinson K, Ulrich JD, Young KL, Robinette ML, Gilfillan S, Krishnan GM, Sudhakar S, Zinselmeyer BH *et al* (2015) TREM2 lipid sensing sustains the microglial response in an Alzheimer's disease model. *Cell* 160: 1061 – 1071
62. Huang WC, Yen FC, Shie F-S, Pan C-M, Shiao Y-J, Yang C-N, Huang F-L, Sung Y-J, Tsay H-J (2010) TGF-β1 blockade of microglial chemotaxis toward Aβ aggregates involves SMAD signaling and down-regulation of CCL5. *J Neuroinflammation* 7: 11
63. Turnbull IR, Gilfillan S, Cella M, Aoshi T, Miller M, Piccio L, Hernandez M, Colonna M (2006) Cutting edge: TREM-2 attenuates macrophage activation. *J Immunol* 177: 3520 – 3524
64. Benjamini YHY (1995) Controlling the false discovery rate: a practical and powerful approach to multiple testing. *J R Stat Soc Series B* 57: 289 – 300
65. Schindelin J, Arganda-Carreras I, Frise E, Kaynig V, Longair M, Pietzsch T, Preibisch S, Rueden C, Saalfeld S, Schmid B *et al* (2012) Fiji: an open-source platform for biological-image analysis. *Nat Methods* 9: 676 – 682
66. Holtmaat A, Bonhoeffer T, Chow DK, Chuckowree J, De Paola V, Hofer SB, Hubener M, Keck T, Knott G, Lee WC *et al* (2009) Long-term, high-resolution imaging in the mouse neocortex through a chronic cranial window. *Nat Protoc* 4: 1128 – 1144
67. Berriz GF, King OD, Bryant B, Sander C, Roth FP (2003) Characterizing gene sets with FuncAssociate. *Bioinformatics* 19: 2502 – 2504

